JOURNAL OF GEOPHYSICAL RESEARCH, VOL. 114, XXXXXX, doi:10.1029/2009JD011807, 2009

Modulation in interannual sea ice patterns in the Southern Ocean in association with large-scale atmospheric mode shift

Yusuke Udagawa,[1] Yoshihiro Tachibana,[2,3] and Koji Yamazaki[4]

Received 27 January 2009; revised 30 July 2009; accepted 10 August 2009; published XX Month 2009.

[1] We verified that the synchronous propagations of the spatial patterns of sea ice concentration (SIC) of wave number 2 around the Antarctic occurred only for the period 1984 to 1994. An empirical orthogonal function (EOF) analysis of satellite data for 1979–2003 objectively demonstrates that the spatial pattern of SIC propagated eastward only in 1984–1994; in other years, it did not. Our results show that interannual variations in SIC patterns are associated with differences in the dominant large-scale atmospheric patterns. In nonpropagating years, variance of the tropospheric Antarctic oscillation (AAO) predominated. However, in propagating years, the AAO variance was subdominant to that of the Pacific South American (PSA) teleconnection pattern having a 4 year period. Such periodic PSA enables the SIC anomalies to propagate eastward with a periodically reinforced dipole pattern. The shift of large-scale atmospheric variability is one possible cause of the modulation in the SIC pattern. The switch of the atmospheric EOF leading mode from the PSA pattern to the AAO in the mid-1990s corresponded to the modulation in the SIC pattern and supports the presence of the atmospheric climate shifts.

Citation: Udagawa, Y., Y. Tachibana, and K. Yamazaki (2009), Modulation in interannual sea ice patterns in the Southern Ocean in association with large-scale atmospheric mode shift, *J. Geophys. Res.*, *114*, XXXXXX, doi:10.1029/2009JD011807.

1. Introduction

[2] Previous studies have presented two views of circum-Antarctic interannual climatic variation. One view involves the Antarctic circumpolar wave (ACW) and eastward synchronous propagation of the spatial patterns of sea ice extent, sea surface temperature (SST), sea level pressure (SLP), and meridional wind stress anomalies with wave number 2 around the Antarctic [e.g., *White and Peterson*, 1996; *Motoi et al.*, 1998]. The atmospheric wave is also characterized by eastward propagation. Additionally sea surface height (SSH) anomalies in the Southern Ocean synchronously propagate eastward with the SST in association with the ACW, and the ocean plays an important role in creating and maintaining the ACW [*Jacobs and Mitchell*, 1996]. Moreover, maintenance of the ACW involves coupling between ocean and atmosphere. [*Qiu and Jin*, 1997; *White et al.*, 1998]. It is a remarkable example of self-organization between the global ocean and the atmosphere. In contrast, the other view proposes that the circum-Antarctic climate is governed by a geographically phase-locked quasi-stationary wave in sea ice, SST, and surface air temperature, which is linked to the El Niño–Southern Oscillation (ENSO) variability [e.g., *Yuan and Martinson*, 2000, 2001; *Kwok and Comiso*, 2002, *Kidson and Renwick*, 2002; *Renwick*, 2002; *Yuan*, 2004]. This quasi-stationary wave is known as the Antarctic Dipole (ADP) [*Yuan and Martinson*, 2000, 2001]. It is characterized by an out-of-phase relationship between these anomalies in the central/eastern Pacific and Atlantic sectors of the Antarctic. The dipole consists of a strong standing mode with weak eastward propagation. The Antarctic sea ice distribution is formed and maintained by an atmospheric stationary or standing wave train that amplifies in association with atmospheric blocking over the South Pacific [*Renwick and Revell*, 1999]. The stationary wave train associated with the blocking is caused by the propagation of atmospheric Rossby waves activated by ENSO [*Karoly*, 1989; *Trenberth et al.*, 1998; *Kidson*, 1999; *Mo*, 2000; *Cai and Watterson*, 2002; *Kidson and Renwick*, 2002] and is named the Pacific South American (PSA) teleconnection pattern [*Mo and Ghil*, 1987]. *Cai and Watterson* [2002] also demonstrated that ENSO forcing amplifies the PSA along with amplification by internal atmospheric dynamics.

[3] *Park et al.* [2004] showed that most of the Antarctic interannual variability can be explained by a geographically phase-locked standing wave train linked to tropical ENSO episodes using a Fourier decomposition into stationary and propagating components of several oceanic and atmospheric variables (i.e., SST, SSH, and SLP). Although their work involved the two views of circum-Antarctic interannual climatic variation, they did not include sea ice variability. To harmonize these different views and clarify the circum-

[1]Graduate School of Environmental Science, Hokkaido University, Sapporo, Japan.
[2]Research Institute for Global Change, JAMSTEC, Yokosuka, Japan.
[3]Climate and Ecosystem Dynamics Division, Faculty of Bioresources, Mie University, Tsu, Japan.
[4]Faculty of Environmental Earth Science, Hokkaido University, Sapporo, Japan.

0148-0227/09/2009JD011807$09.00

Antarctic interannual climatic variations, sea ice studies, especially relating to its interannual variability, are helpful because sea ice functions as an interface between the ocean and the atmosphere and is influenced by both. Present study will demonstrate the spatial and temporal variations of sea ice using newly available passive microwave satellite data for 1979–2003.

[4] Although numerous previous studies have described sea ice variability in the Southern Ocean in association with atmospheric surface conditions such as the SLP and wind stresses, many have not discussed the relationship between sea ice and the whole troposphere. *Bonekamp et al.* [1999] and *Connolley* [2002], who demonstrated that propagation of the SLP anomaly, i.e., ACW signal, is only present in the period of 1985–1994, have also made a remarkable contribution in trying to harmonize the different views. However, their atmospheric analysis did not include the whole troposphere, but rather was restricted to air in direct contact with the ocean. The action centers of interannual atmospheric variability are usually located in the middle or upper troposphere, rather than in the lower troposphere [*Thompson and Wallace*, 2000]. An example of tropospheric variation is the Southern Hemisphere annular mode or the Antarctic oscillation (SAM/AAO) [*Thompson and Wallace*, 2000] in which the AAO connects even to the stratosphere. The PSA pattern appears in the middle or upper troposphere, but the center of action of sea ice is in the lower troposphere. Therefore a better understanding of long-term whole tropospheric circulation in association with our long-term sea ice analysis should help clarify the Antarctic climate system. The knowledge about Antarctic climate system can go one step further by looking at both of sea ice and whole tropospheric circulation.

[5] We will address a new theory/hypothesis of circum-Antarctic interannual climatic variations by focusing on sea ice variations as revealed by statistical analyses of long-term, satellite-derived sea ice data and atmospheric reanalysis data. *Bonekamp et al.* [1999] have pointed out the possibility of a regime shift in sea ice variability in the Southern Ocean, but its cause has not yet been understood. In this study, we will demonstrate that shift of atmospheric variation controls whether the sea ice propagates eastward or not. In other words, the replacement of dominant atmospheric patterns modulates the sea ice variability.

[6] Data sets and the statistical methods used in this study are described in sections 2 and 3, respectively. Results are described in section 4, and discussion and concluding remarks are in sections 5 and 6, respectively.

2. Data

[7] Monthly sea ice concentration (SIC) data provided by the Oceans and Ice Branch, Laboratory for Hydrospheric Processes at NASA Goddard Space Flight Center (GSFC, NASA team algorithm) were used to investigate the interannual variability of sea ice in the Southern Ocean. The SIC data are derived from the Nimbus 7 Scanning Multichannel Microwave Radiometer (SMMR) and the Defense Meteorological Satellite Program (DMSP)-F8, -F11, and -F13 Special Sensor Microwave/Imagers (SSMIs). These two sets of satellite data were combined by *Cavalieri et al.* [1996, 1997], and the combined data set is available for the period of 1979–2003 with a spatial resolution of 25×25 km. This data set is available from http://nsidc.org/data/nsidc-0051.html, and includes gridded daily and monthly averaged sea ice concentrations for both the north and the south polar regions. Two types of data are provided, final data and preliminary data. Final data are produced at GSFC about once per year. Preliminary data are produced at The National Snow and Ice Data Center (NSIDC) approximately every three months and include roughly the most recent three to twelve months of processed data. The data we used is the final data, which includes additional quality control, including temporal interpolation of large data gaps in the daily data. Additionally particular care is needed to interpret the sea ice concentrations during summer when the melt is present and in regions where new sea ice makes up a substantial part of the sea ice cover. Some residual errors remain due to weather effects, mixing of ocean and land area in the sensor field of view, and the differences of sensors. It is recommended that sea ice extent and area computed from daily maps of sea ice concentrations be used to compute monthly averages of those parameters. In this paper, we use monthly means on winter seasons, and so this error will not impact our analyses.

[8] We also used monthly optimal interpolation sea surface temperature (OISST, hereafter SST) data compiled by the National Oceanic and Atmospheric Administration (NOAA) on a 1.0×1.0 degree regular latitude–longitude global grid [*Reynolds and Smith*, 1994] and daily mean atmospheric reanalysis data provided by the National Centers for Environmental Prediction/National Centers for Atmospheric Research (NCEP/NCAR) [*Kalnay et al.*, 1996] on a 2.5×2.5 degree regular latitude–longitude global grid. The analysis period for all of the data sets was 1979 through 2003. The NCEP/NCAR reanalysis data set, which is referred to as the NCEP1 data, was obtained from the National Weather Service Climate Prediction Center reanalysis project (available online at http://www.ncep.noaa.gov/cdc/reanalysis/reanalysis.shtml). We use 10m wind data in order to calculate the curl of the wind stress along with geopotential height and temperature data at standard levels. For detailed calculations, see section 3.

[9] *Bromwich and Fogt* [2004] concluded that, for austral nonsummer climate studies across Antarctica and the Southern Ocean, neither ECMWF (European Centre for Medium-Range Weather Forecasts) 40 Year Re-analysis (ERA-40) data nor NCEP1 data are reliable prior to the modern satellite era (before 1979), because the frequency of ship-based observations in coastal Antarctica, which help to constrain the reanalysis, decreases during winter. Also, *Tennant* [2004] pointed out that NCEP1 has areas of sparse data coverage in the South Pacific and South Atlantic Oceans, and concluded that NCEP1 is not reliable during any season prior to 1979 in the Southern Hemisphere. *Bromwich et al.* [2007] presented a wide review of recent knowledge regarding the status of the major global reanalyses in the polar regions. They concluded that the beginning of the modern satellite era in 1979, when new quantities of data were assimilated for the first time, created a sudden adjustment in the Southern Ocean and Antarctica. Additionally, there was a problem in assimilating bogus surface pressure observations in NCEP1 in Southern Hemisphere, known as the PAOBS problem (see online at http://www.cpc.ncep.noaa.gov/products/wesley/paobs/paobs.html). This error affects 1979–1992 (14years) in the

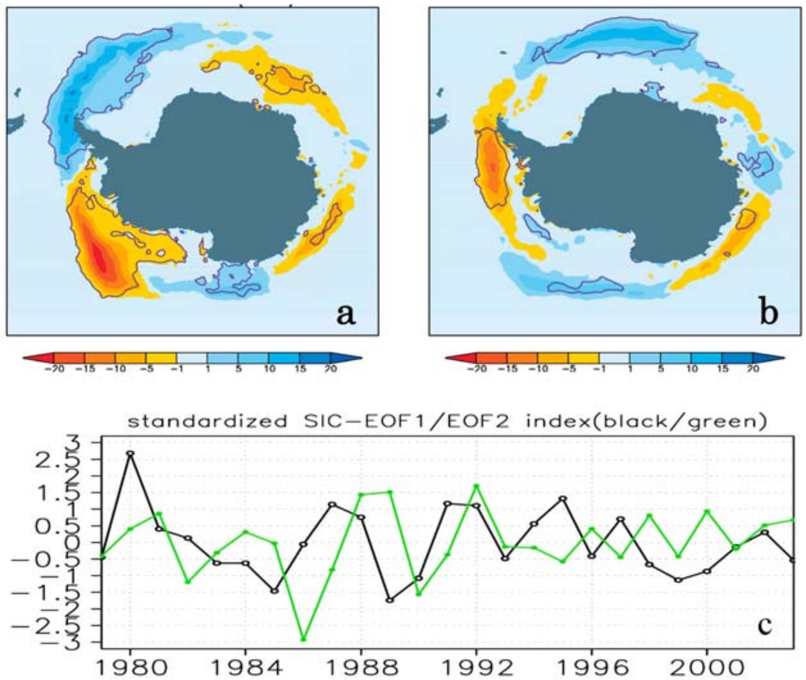

Figure 1. Spatial patterns of the (a) first and (b) second modes of JASO mean SIC anomalies around the Antarctic for 1979–2003. (c) Corresponding time series of the first (black line) and second (green line) modes. The indices are standardized. The shading in Figures 1a and 1b indicates linear regression coefficients of the SIC with the time series of the first and second mode, respectively (unit is %). The gradation of the shading changes in increments of 5%, but absolute values <1% are ignored. The contours indicate 95% statistical confidence based on t tests.

40°S–60°S band on daily to weekly timescales. In this paper, we use monthly means on pressure levels, and so this error will not impact our analyses. As discussed above regarding the uncertainty of reanalysis data sets before satellite era, we mainly use the reanalysis data sets from the satellite era (1979). Therefore, this problem will not impact our study.

3. Method

[10] Wintertime seasonal averages of the SIC, SST, and atmospheric data were mainly used, with winter defined as July, August, September, and October (JASO) for SIC, and July, August, and September (JAS) for SST and atmospheric data. As there may be some lag in the response of sea ice with large inertia to winter atmospheric variation, we have included October in the winter season only for the SIC data analysis. An empirical orthogonal function (EOF) analysis was applied to the covariance matrix of the winter-averaged SIC anomalies. The spatial coverage of the SIC-EOF analysis was the entire area of sea ice around the Antarctic (from approximately 40° S to 90° S). The JASO mean data are used for the SIC-EOF calculation. We also applied an atmospheric EOF analysis to mass-weighted vertical average geopotential height anomaly data from 1000 to 300 hPa for the extraction of the dominant barotropic components. Note that there was not much difference between the result of analysis for the vertical averaged data and for the 500 hPa data. Additionally, geopotential height data were weighted by area using the square root of the cosine of latitude to ensure equal area weighting for the covariance matrix. The atmospheric EOF analysis covered an area from 20 degrees S to 90 degrees S so that a leading teleconnection pattern in the extratropic atmospheric circulation could be identified.

[11] Temperature advection and the curl of wind stress were calculated for each day using the daily NCEP1 data. Data from 925 hPa were used to calculate temperature advection, and 10 m wind data were used to calculate wind stress. JAS and climatological means were then calculated.

4. Results

4.1. Sea Ice Variability

[12] Figure 1 shows the spatial SIC patterns of the first and second modes of the EOF (referred to as SIC-EOF1 and SIC-EOF2, respectively) and their PC scores. The analysis covered the period of 1979–2003. The SIC-EOF1 exhibits positive anomalies in the western Atlantic and western Pacific sectors, but negative anomalies in the Amundsen Sea, Ross Sea, the western Indian Ocean, and eastern Indian Ocean sectors. This spatial pattern looks like the Antarctic Dipole (ADP) [*Yuan and Martinson*, 2000, 2001; *Yuan*, 2004]. The SIC-EOF2 shows positive anomalies in the eastern Atlantic sector and central Pacific sector, but negative anomalies in the Bellingshausen Sea and the eastern Indian Ocean sector. The spatial patterns of both EOFs have wave number 2 and variances of 25.8% and 14.3%, respectively. SIC-EOF2 resembles SIC-EOF1, with the spatial pattern of SIC-EOF2 appearing to shift eastward by about 45 degrees relative to that of SIC-EOF1. The interannual variation of the PC1 score also shows a striking resemblance to that of the PC2 score, but with a roughly 1 year lag, especially during 1984 to 1994. These results indicate that the EOF decom-

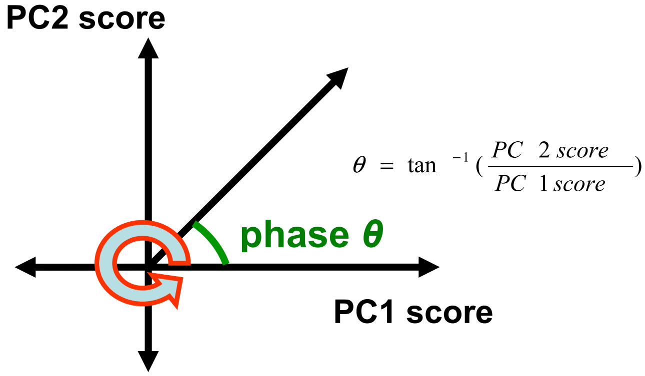

Figure 2. Schematic map showing the relationship between the indices (PC1 and 2 scores) of the two leading SIC-EOFs and the phase, θ. Counterclockwise rotation of θ with time defines the increment in θ. Thus, in the period in which θ increases (decreases), the SIC anomalies propagate eastward (westward).

posed an easterly propagating mode into the two standing modes. To confirm this, we examined the lag correlation of the PC scores. The simultaneous correlation coefficient is, by definition, zero. The correlation with a 1 year lag (lead) results in a coefficient of 0.57 (−0.48), which exceeds the 99% significance level based on t tests. The correlation coefficient for a 2 year lag (lead) is −0.14 (−0.06).

[13] These results indicate that the year of the prominent EOF2 spatial pattern tends to occur 1 year after the year of the prominent EOF1 spatial pattern. One year after the year of prominent EOF2, the EOF1 spatial pattern with negative sign occurs. The same pattern with the negative sign then repeats, with the prominent EOF1 spatial pattern reoccurring 4 years later. Therefore the sea ice spatial pattern with wave number 2 tends to propagate eastward in a 4 year period.

[14] The PC scores are by definition orthogonal. To verify the rotation of the SIC spatial pattern, viewing the pattern from the polar coordinates is more advantageous than from the Cartesian coordinates (Figure 2). We viewed the two components based on their amplitude and the phase of interannual SIC variability. We defined the phase, θ, as

$$\text{phase } \theta = \tan^{-1}\left(\frac{PC2score}{PC1score}\right)$$

When the phase θ rotated counterclockwise in the field of Figure 2, i.e., increases with time, the SIC propagates eastward.

[15] Figure 3 shows the time evolution of the phase θ. Clearly, θ constantly increased with time only between 1984 and 1994, indicating that the SIC anomalies propagated eastward continuously in this period. The average slope of that increment signifies a rotation cycle of about 4 years. However, for the other years, θ did not continuously increase with time. Thus, the SIC anomalies did not propagate eastward from 1979 to 1984 or from 1994 to 2003. Figure 3 demonstrates that the spatial pattern of SIC anomalies with wave number 2 propagated eastward only from 1984 to 1994. The ADP is composed of a standing mode with weak eastward propagation [*Yuan and Martinson*, 2000, 2001; *Yuan*, 2004]. Our results show that the dipole structure is present, but also clearly show that it propagates eastward in the 1984–1994 period, meaning that during this period it is more reasonable to regard the sea ice variation as a visualization of a propagation signature by the Antarctic circumpolar wave (ACW) than to regard it as a visualization of a standing signature of the ADP. The period is the same as that shown by *White and Peterson* [1996]. However, the signal is clear only in the west Antarctic. Therefore, strictly speaking, this signal is not exactly the same as the ACW. Also, our results are consistent with *Connolley* [2002], in which the ACW was evident only from 1985 to 1994 using data analysis from 1968 to 1999. However, he did not determine why the ACW was prominent only in that period, but simply speculated that it may be due to an external forcing, such as ENSO, or intrinsic atmospheric variation. We will focus on discovering why the SIC anomaly only propagates eastward in the years 1984–1994.

4.2. Atmospheric Variability

[16] Because the spatial SIC pattern during 1984–1994 differed from that in other years, the atmospheric variations that forced the sea ice in those years may also have differed. In this subsection, we focus on differences in large-scale atmospheric patterns in association with the modulation in sea ice variation. However, first, we describe the overall dominant atmospheric variations over and around the Antarctic from 1979 to 2003. Figure 4 shows the first and second EOFs of atmospheric spatial patterns and their corresponding time series. Hereafter, the spatial pattern of the atmospheric first mode and its time series are referred to as the ATM EOF1 and ATM EOF1 index (PC1 scores), respectively, and those of the second mode as the ATM EOF2 and ATM EOF2 index (PC2 scores). The variances contributed by ATM EOF1 and ATM EOF2 are 29.7% and 18.6%, respectively. We used the whole troposphere average for the analysis. This can filter out the variability that appears only within the lower troposphere. The spatial pattern of the first mode is similar to that of the AAO [*Gong and Wang*, 1999]/SAM [*Thompson and Wallace*, 2000], whereas the second mode exhibits positive anomalies in the western Atlantic sector and negative anomalies in the central Pacific sector. The second mode is similar to that shown by *Karoly* [1989], *Cai and Baines* [2001], and *Cai*

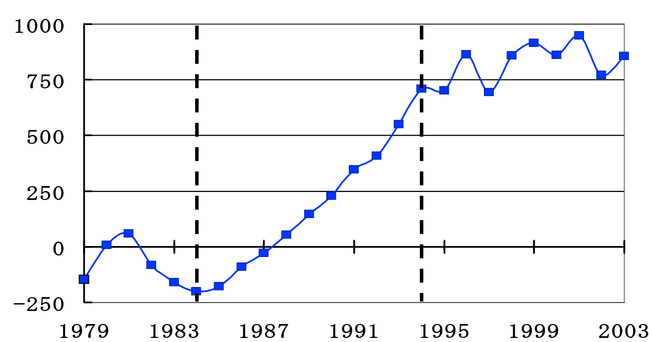

Figure 3. Year-to-year evolution of the phase, θ. Horizontal and vertical axes show the year and the phase, respectively (phase unit = degrees). To illustrate the rotational status schematically, even if the phase value exceeds 360 degrees, we did not reset the phase to zero.

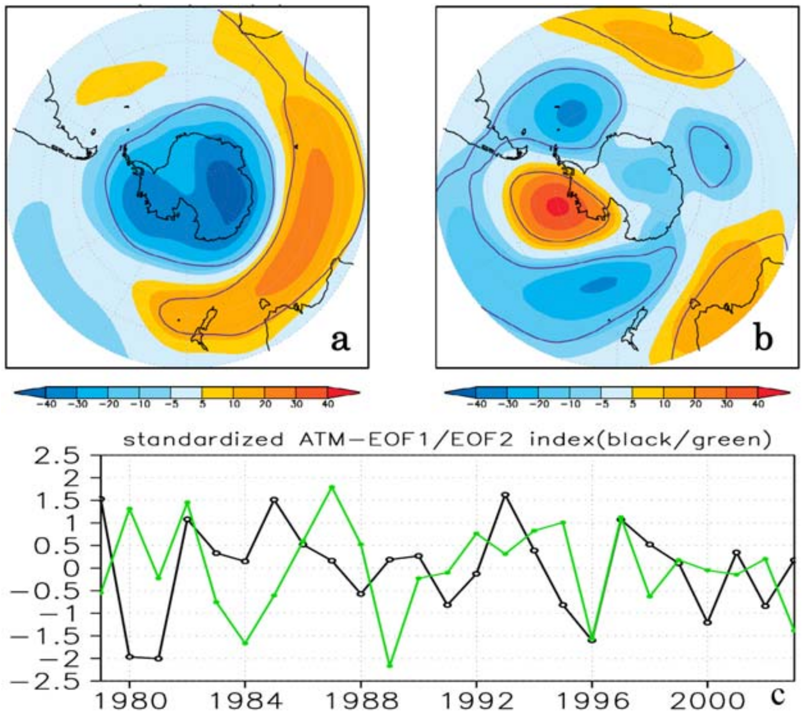

Figure 4. The spatial patterns of (a) ATM EOF1 and (b) ATM EOF2 for the JAS mean vertically integrated geopotential height anomalies from 20° S to 90° S for 1979–2003. See the text for details on the calculation method. (c) Corresponding time series of the first (black line) and second (green line) modes. The values are standardized. Shading in Figures 4a and 4b indicates the linear regression coefficients for the mass-weighted, vertically integrated geopotential height field with the time series of the first and second modes, respectively. The unit for the shading is meters. The gradation of the shading changes every 10 m, but absolute values <5 m are ignored. The contours indicate 95% statistical confidence based on *t* tests.

and Watterson [2002]. In these studies, the largest variability with respect to the 200 hPa [*Karoly*, 1989] and 500 hPa geopotential height was in the Pacific sector, with the second largest peak in the western Atlantic sector; this pattern reflects a geographically phase-locked standing wave. Significant action centers of our ATM EOF2 in the western Atlantic sector, the Bellingshausen–Amundsen Seas, and the east South Pacific, i.e., to the south of New Zealand, agree with those described in these articles. This is the so-called PSA pattern, which is activated by tropical anomalous heating [*Hoskins and Karoly*, 1981; *Karoly*, 1989]. *Mo and Ghil* [1987] discovered and defined the PSA pattern for the first time. They define the second and third EOFs of 500 hPa geopotential height anomaly as the PSA pattern. Their PSA pattern has the strongest signature centered on the Antarctic Peninsula. Our third EOF (figure is not shown) does not have such a feature as theirs, and the corresponding contribution is as small as 11.9%. We therefore adopt our EOF2 as the PSA pattern. As shown in Figure 4b, the strongest signature can be seen near the Antarctic Peninsula. The amplitude of the ATM EOF1 index (PC1 scores) for 1984–1994 appears to be smaller than that for other periods, whereas the amplitude of the ATM EOF2 index (PC2 scores) for 1984–1994 appears larger. Table 1 also suggests these changes in variance. These results indicate the change/shift of large-scale atmospheric variations.

4.3. Atmospheric Variation From 1984 to 1994

[17] If atmospheric factors cause the modulation in SIC variation, there must be some signatures that differentiate the SIC variation in large-scale atmospheric patterns. To identify the atmospheric patterns that modulate the SIC, we separately calculated atmospheric first and second EOFs for the period 1984–1994 and for other years. We first show the atmospheric variation, i.e., the atmospheric geopotential height field, only in 1984–1994, based on the same atmospheric EOF analysis as described above. Figure 5 shows the spatial patterns of the first and second modes and their corresponding time series. The first and second modes contribute 28.7% and 25.0% of the variance, respectively. The time variation of the first mode is obviously cyclic with an approximately 4 year period. Further, the wavy structure of the first mode spatial pattern is quite similar to that of the

Table 1. Variances of the Time Series of Atmospheric EOFs in the Subperiods From 1984 Through 1994 and in Other Subperiods[a]

Index	1984–1994	1979–1983 and 1995–2003
ATM-EOF1	0.553	1.363
ATM-EOF2	1.311	0.914

[a]ATM-EOF1 and ATM-EOF2 represent the first and second modes, respectively, of the atmospheric EOF. The SIC anomalies were characterized by eastward propagation in 1984–1994. In the other years, the SIC anomalies did not have any features of eastward propagation.

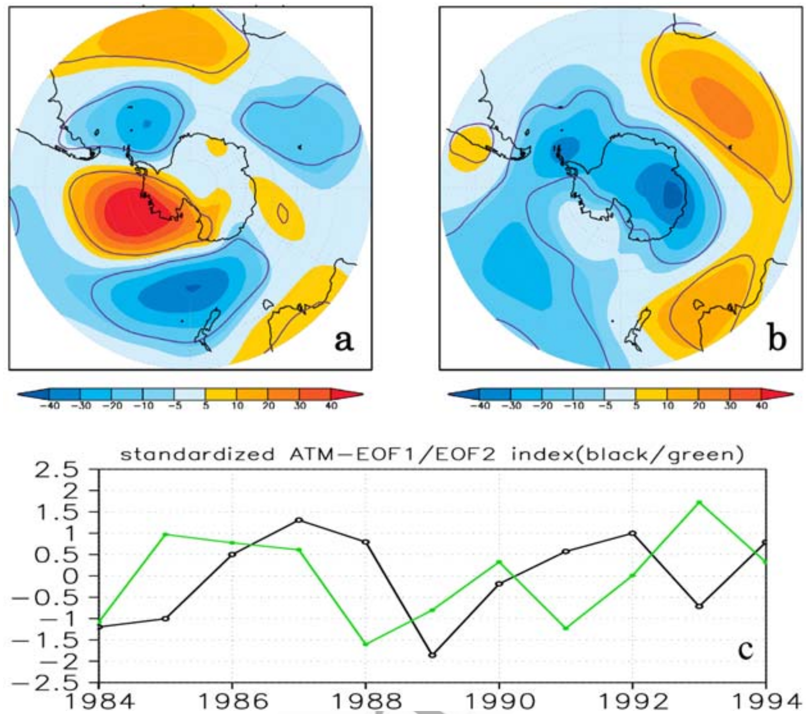

Figure 5. The same as Figure 4, except for the EOF calculation only for the period of 1984–1994.

second mode for the whole period (Figure 4b). The correlation coefficient between the first mode time series in this subperiod and the second mode time series in the whole period is 0.90. In this subperiod, the second mode is not similar to the first mode calculated for the whole period. Thus, in this subperiod, the PSA pattern was dominant as the first mode. The approximately 4 year cycle of the first mode, i.e., the PSA pattern, coincides with the period of the eastward propagation of the SIC. This coincidence suggests that the atmospheric shift should change/modulate the pattern of SIC variation. Hereafter, we define the normalized time series of the first-mode EOF for 1984–1994 as the PSA index (PC1 scores) and investigate the influence of the PSA on eastward SIC propagation. Note that we normalize the time series divided by the standard deviation and the definition of the positive PSA pattern in this paper is the pattern like Figure 5a. Although the time series of the PSA index (PC1 scores) is 10 years long, an approximately 4 year cycle is resolvable. Therefore, the variance of a cyclic PSA pattern with an approximately 4 year cycle was predominant in the atmosphere in the period 1984–1994.

4.4. Atmospheric Variation From 1979 to 1983 and 1995 to 2003

[18] Here, we focus on atmospheric variations in the subperiods 1979–1983 and 1995–2003, when SIC anomalies did not propagate eastward, using the same atmospheric EOF analysis. The spatial patterns of the first mode and the second mode and their corresponding time series are shown in Figure 6. The spatial patterns of both are quite similar to those of the first and second modes for the whole period shown in Figure 4. These modes again exhibit the AAO pattern and the PSA pattern, respectively. The variances contributed by the leading and second modes are 38.9% and 17.9%, respectively. The first mode (i.e., the AAO) is more predominant than that for the whole period. In addition, the spatial pattern of the second mode in Figure 6b is quite similar to that of the first mode for the period 1984–1994, shown in Figure 5a, which exhibits the PSA pattern. The variances for Figures 6b and 5a are 17.9% and 28.1% respectively. This difference indicates that the PSA was damped in the periods 1979–1983 and 1995–2003 compared to the period 1984–1994. It is possible that the leading modes shown in Figure 6 are not real as disjointed time series were combined for use in an EOF analysis. To confirm the modes in Figure 6 are real, we performed the EOF analysis on the individual time periods i.e., 1979–1983 and 1995–2003 separately (figures not shown). The spatial patterns of these individual EOF analyses show the AAO and PSA patterns as first and second modes respectively, corresponding to Figures 4 and 6. The time series of the individual EOFs were also similar to those in Figures 4 and 6 for both periods 1979 to 1983 and 1995 to 2003. Therefore, we consider the EOF results shown in Figure 6 to be valid.

5. Discussion

[19] We determined a number of characteristics of large-scale atmospheric variability associated with sea ice variability. The spatial pattern of sea ice with wave number 2 propagated eastward only in 1984–1994. In other years, no significant eastward propagating features were signified. Differences in large-scale dominant atmospheric patterns were also uncovered. In the nonpropagating years, the AAO variance predominated. In years of eastward SIC propagation, the variance of a cyclic PSA pattern with an approximately 4 year cycle was predominant in the atmosphere.

[20] Below, we examine the cause of the SIC modulation. We first describe the external forcing of the PSA pattern that

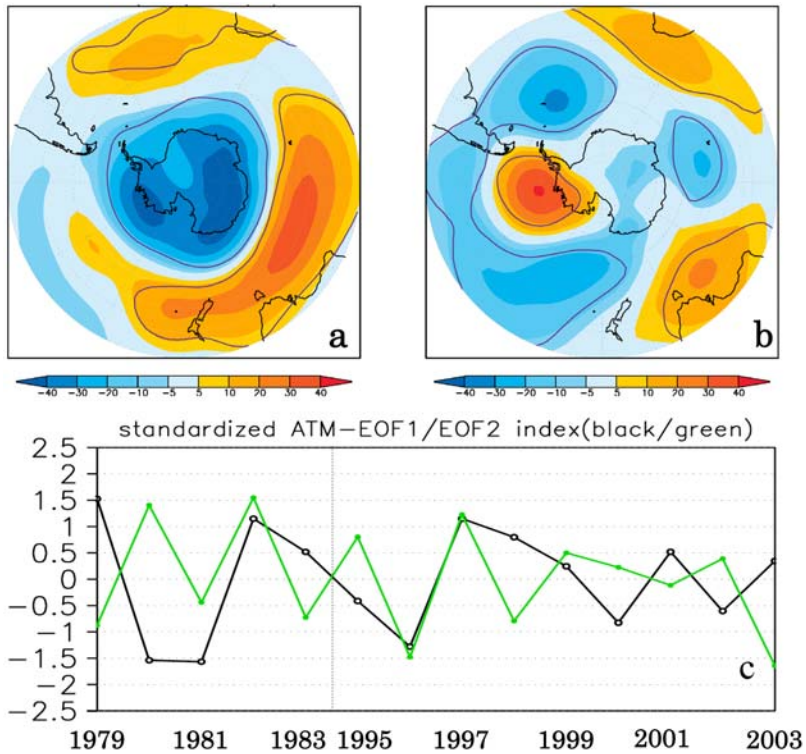

Figure 6. The same as Figure 4, except for the EOF calculation only for 1979–1983 and 1995–2003. The variances contributed by the EOF1 and the EOF2 are 38.9% and 17.9%, respectively.

causes the eastward propagation of the SIC. We then discuss the shift of atmospheric variation that determines the modulation in SIC variation.

5.1. Propagation of the SIC and Atmospheric PSA Pattern

[21] Figure 7 shows simultaneous and lagged regression patterns of the SIC with the atmospheric PSA index (PC1 scores); each of the simultaneous, 1 year, and 2 year lagged SIC patterns has a wave number of 2. Figure 7a shows an area of large negative (positive) variability over the central Pacific sector (the western Atlantic sector). This spatial pattern is quite similar to that of SIC-EOF1. In fact, the PSA index (PC1 scores) and SIC-EOF1 PC score have a correlation coefficient of 0.88 for the period of 1984–1994. The PSA index (PC1 scores) is the time series of the first EOF executed only in 1984–1994. Also, Figure 7 clearly shows that the areas of large positive and negative regression propagated eastward year by year. Therefore, the PSA pattern somehow forced SIC anomalies to propagate eastward.

[22] Figure 8 shows the relation of atmospheric dynamic and thermodynamic forcing with the PSA index (PC1

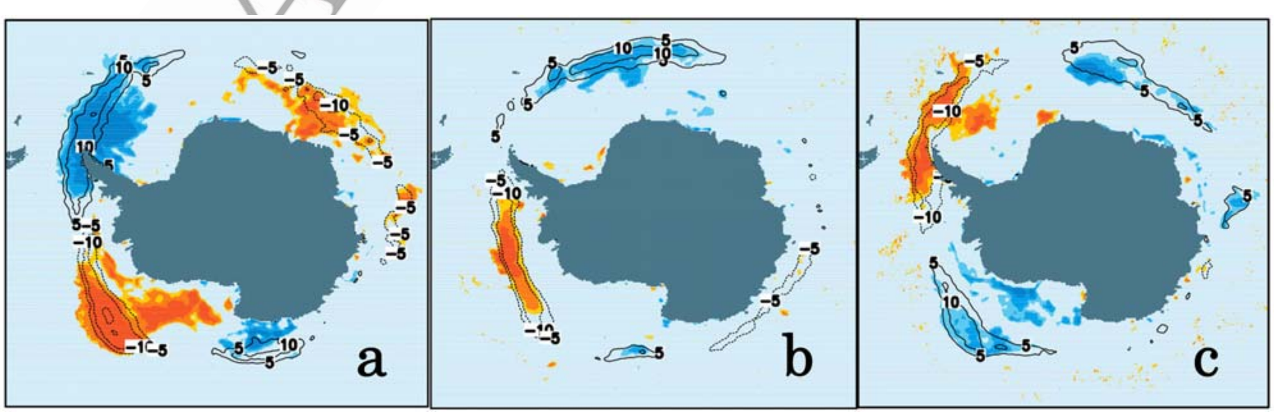

Figure 7. The SIC anomaly field linearly regressed on the standardized PSA index (PC1 scores) of 1984–1994. (a) Simultaneous regressed pattern (1984–1994), (b) 1 year lagged regressed pattern (1985–1995), and (c) 2 year lagged regressed pattern (1986–1996). Gradation of light, moderate, and heavy cold (warm) color shading indicates positive (negative) correlations that respectively exceed 90%, 95%, and 99% statistical significance based on t tests. A positive correlation signifies heavier sea ice than normal. Contours indicate regression coefficients. The unit of the regression coefficient is %.

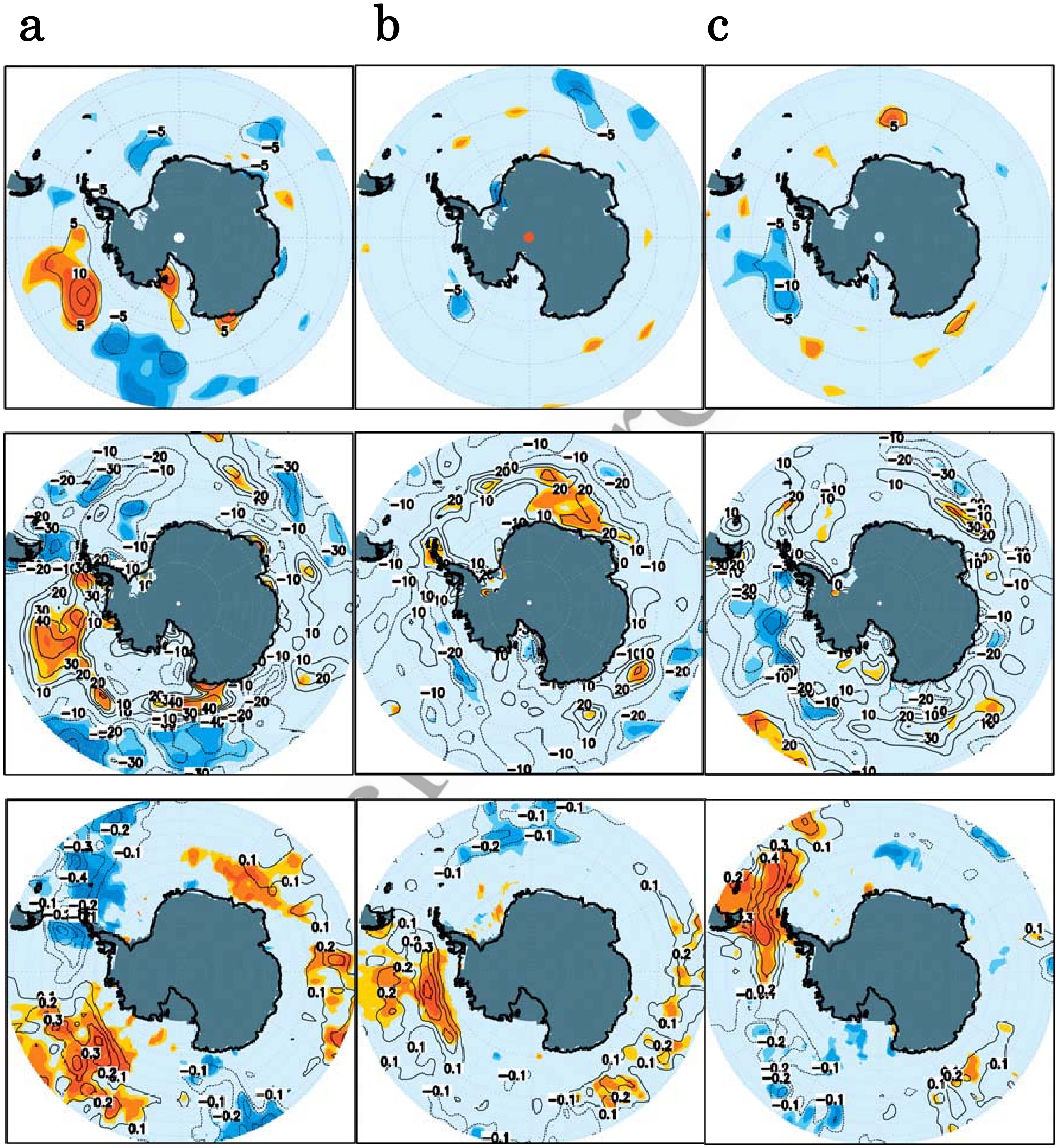

Figure 8. The same as Figure 7, except for (top) the horizontal temperature advection field at 925 hPa, (middle) the curl τ field, and (bottom) the SST anomaly field. The warm color indicates favorable conditions for reductions in sea ice. The units of the regressions at the top, middle, and bottom are, respectively, 10^6 K s^{-1}, 10^9 N m^{-3}, and K.

scores). Simultaneous patterns of temperature advection (Figure 8, top), curl τ (Figure 8, middle), and SST (Figure 8, bottom) commonly show a pair of significant warm and cold anomalies in the central Pacific and Atlantic sectors. The warm (cold) area, which signifies anomalous warm (cold) temperature advection, convergence (divergence) of sea ice, and anomalous warm (cold) SST, is favorable for the decrease (increase) in sea ice. The significant areas of the warm–cold pairs (Figure 8a) agree well with those of the SIC anomalies (Figure 7a). Thus, Figures 7a and 8a indicate that when the index of the PSA pattern (PC1 scores) is large and positive, atmospheric dynamic and thermodynamic external forcing by the PSA pattern amplify the SIC contrast between the central Pacific sector and the Atlantic sector. This atmospheric forcing is favorable for the formation of a dipole of SIC in these sectors. Therefore, the PSA

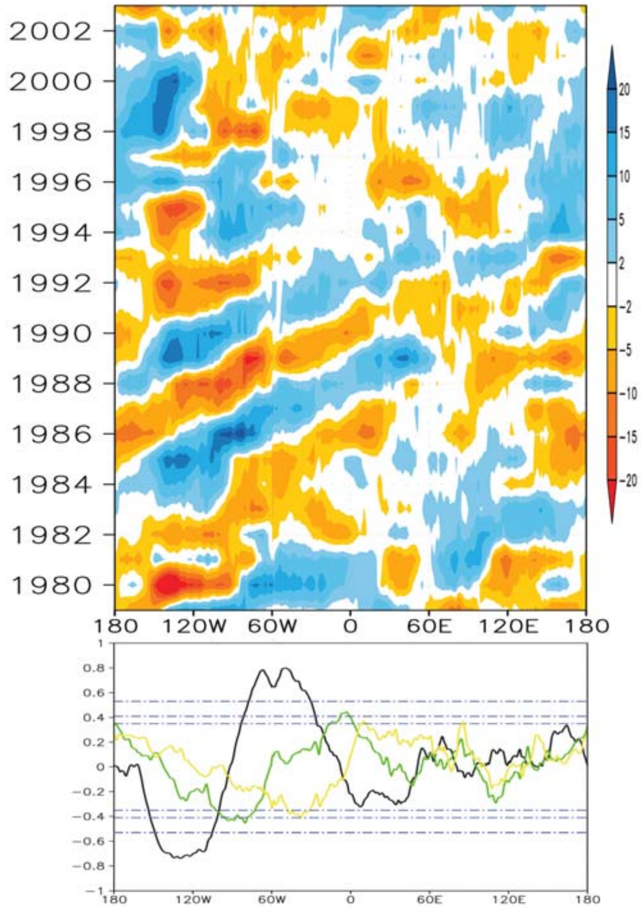

Figure 9. (top) Hovmöller diagram of JASO mean SIC anomalies averaged from 55° S to 70° S around the Antarctic for 1979–2003 (unit is %). (bottom) The meridional mean SIC anomaly averaged from 55° S to 70° S linearly regressed on the standardized ATM-EOF2 index (PC2 scores) of 1979–2003. Simultaneous regressed SIC with respect to the longitude (1979–2003) (black line), 1 year lagged regressed SIC (1980–2002) (green line), and 2 year lagged regressed SIC (1981–2001) (yellow line). Blue dash-dotted lines in the bottom plot indicate 90%, 95%, and 99% statistical significance based on *t* tests.

pattern excites the dipole pattern of the SIC in these areas. The atmospheric forcing 2 years later is in reverse because the index of the PSA pattern (PC1 scores) has a 4 year cycle (Figures 7c and 8c). In other words, the atmosphere periodically forces the formation of an SIC dipole, i.e., Antarctic Dipole [*Yuan and Martinson*, 2000, 2001], every other year with a reversed phase. The atmospheric forcing mostly vanishes 1 year after the year having a large and positive PSA index (PC1 scores, Figure 8b). However, a persistent signature can be seen in the SST field, with positive anomalies in an area approximately 45 degrees eastward from the significant dipole area of the simultaneous SST field. This suggests the presence of eastward movement of the SST signature. Also, the positive and negative SIC patterns located over the western Atlantic and central Pacific sector (Figure 7a) synchronously move eastward 1 year later (Figure 7b). This synchronous SIC and SST propagation was previously discussed by *Martinson* [1993] and *Gloersen and White* [2001]. They demonstrated that the propagating wave of the sea ice variability is carried from one winter to the next winter by the thermal inertia of upper water neighboring the sea ice. The explanation of atmospheric dynamic and thermodynamic forcing with the simultaneous PSA index (PC1 scores) is consistent with *Raphael* [2004, 2007], who examined the relationship between the pattern of an atmospheric zonal wave number three and Antarctic sea ice by using an index of the zonal wave three. The zonal wave three possibly forces an alternating pattern of equatorward (colder) and poleward (warmer) flow, which influences sea ice growth/expansion and decay/retrogression respectively. The basic mechanism underlying the relationship between the atmospheric circulation pattern and sea ice variability via atmospheric dynamic and thermodynamic forcing in our results is consistent with these papers. *Raphael* [2004, 2007], however, did not describe the relationship between the atmospheric zonal wave three and the PSA pattern. The spatial pattern of their atmospheric zonal wave three is different from our PSA pattern deviating/rotating by about 45° with respect to their zonal wave three.

[23] Combining the present results with those of previous studies, we propose the following scenario of eastward rotation of the SIC. The PSA pattern excites the negative and positive dipole structure of the SIC in the central Pacific and western Atlantic sectors in a year with a positive and large PSA index (PC1 scores). The dipole signature is retained in the ocean by large thermal inertia, persisting until the next year. In the following winter, this memorized signature moves eastward in association with the eastward oceanic propagation, as reported by *Martinson* [1993] and *Gloersen and White* [2001]. Two years later, the same atmospheric forcing as in the first year, but with reversed phase, again excites the dipole of the SIC with reversed phase. The memorized signature also moves further eastward toward the opposite side of the Antarctic Peninsula. Three years later, the same oceanic propagation as in the second year, but having the reversed phase, occurs. In the fourth year, the same atmospheric forcing as in the first year once again excites the dipole of the SIC. This 4 year cycle of atmospheric forcing is probably the same as the period of the oceanic signature that rounds the Antarctic. Therefore, this periodic atmospheric forcing excites the dipole, and the ocean makes the dipole signature propagate eastward. In other words, the atmosphere plays a role in creating the dipole, and the ocean plays a role as a carrier of the dipole. The periodicity of this atmospheric forcing is consistent with *Mo* [2000] and *Rasmusson et al.* [1990], who showed that the PSA has a 48 month cycle that is driven by the ENSO. Regarding the Antarctic dipole pattern of sea ice variability, *Holland et al.* [2005] focused on the standing wave pattern in sea ice anomaly associated with simulated Antarctic dipole variability and investigated the mechanisms in detail using a climate coupled model. They showed that the Antarctic dipole pattern of sea ice variability was forced by a combination of both thermodynamics (e.g., ice/ocean surface heat flux convergence analysis) and dynamical processes. Their result is consistent with ours, in particular, with the role of the anomalously high SLP in Figures 4b, 5a, and 6b, in the Amundsen–Bellingshausen Sea.

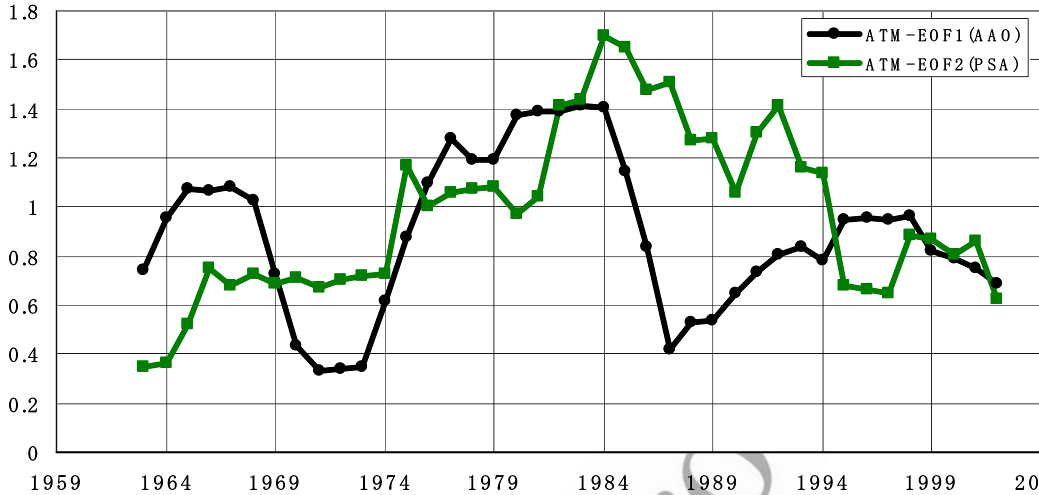

Figure 10. Variances of the time series of atmospheric EOFs on each 11 years between 1958 and 2007. ATM-EOF1 (AAO) and ATM-EOF2 (PSA) denote the variances of the first and second modes, respectively, of the atmospheric EOF in the period from 1958 through 2007.

[24] As shown in Figures 7 and 8, the eastward propagation seems to only be visible over the western part of the Southern ocean. To confirm this, we show that the Hovmöller (longitude-time) diagram of JASO mean SIC anomalies averaged from 55° S to 70° S around the Antarctic for 1979–2003 (Figure 9, top). Figure 9 (top) clearly demonstrates that the signal of eastward propagation is only evident from 180° W to 60° E. Figure 9 (bottom) shows the simultaneous and lagged correlation of JASO mean SIC, averaged from 55° S to 70° S around the Antarctic for 1979–2003, along with the ATM-EOF2 index (PC2 scores) in the period 1979–2003 (as the atmospheric PSA index). Each of the simultaneous (black line), 1 year (green line), and 2 year (yellow line) lagged SIC patterns have two peaks that satisfy the statistical significance criteria. Blue dash-dotted lines indicate 90%, 95%, and 99% statistical significance based on t tests, respectively. The simultaneous correlation pattern exhibits large negative and positive values over the area of 120° W, or the central Pacific sector, and the area of 60° W, or the western Atlantic sector. This spatial correlation pattern signifies the Antarctic dipole. In addition, the lag correlation lines clearly show that the areas of large positive and negative correlation coefficients propagated eastward year by year only over 180° W to 60° E. *Yuan and Martinson* [2000] indicated that the Antarctic dipole consists of a strong standing mode with a very weak propagating signature. As shown in Figure 9, however, we can demonstrate that in the period 1984–1994, the Antarctic dipole has a standing mode with a substantially strong propagating motion compared with other periods i.e., nonrotating years.

5.2. Nonpropagation of the SIC and Atmospheric AAO

[25] Here, we propose an explanation for the SIC change/modulation. We calculated the horizontal temperature advection field, the curl τ field, and the SST anomaly field linearly regressed over the time series of the second EOF executed in the subperiods of nonrotation, as in Figure 6. Signatures that may induce eastward propagation of the SIC could not be seen in any of the fields (figures not shown). Also, Figure 9 (top) shows no propagating signature of the SIC in these subperiods. In addition, a 4 year cycle was not dominant in the time series of the second mode in the subperiods of nonrotation (see Figure 6). The variance of the PSA in the subperiods of nonrotation was, moreover, smaller than that in the subperiod of rotation. In fact, the AAO overwhelmed the PSA pattern in the subperiods of nonrotation. This weak atmospheric external forcing made the formation of the dipole pattern of the SIC difficult. The fact that 4 year cyclic atmospheric forcing was not dominant also reduces the possibility of propagation of the SIC. Therefore, the shift of the dominant atmospheric pattern is quite important for determining whether the SIC propagates. In the nonrotating subperiods, the AAO pattern was predominant, whereas in the rotating period, the AAO pattern was subdominant.

5.3. Shift of the Dominant Atmospheric Pattern

[26] As discussed above, the shift of the dominant atmospheric pattern is quite important for determining whether the SIC propagates. In this subsection, we focus on the shift/change of the dominant atmospheric pattern for longer time period. To identify the shift of the atmospheric patterns over a longer time period, we calculated atmospheric first and second EOFs for the period 1958–2007 based on the same atmospheric EOF analysis as described in Section 4.2 (figures not shown). The spatial pattern and corresponding time series of the first (second) mode are quite similar to those of the AAO (PSA) mode, as shown in Figure 4. Although the analysis period includes the era with no satellite data, i.e., before 1979, we consider that the patterns are realistic and have physical meaning because these patterns are similar to those of the period 1979–2003. We further calculated variances for each 11 year period for the time series of atmospheric EOFs in the period 1958–2007. The variance lines are shown in Figure 10; for example, the value in 1990 signifies the variance in the period 1985–1995. The variances of the PSA pattern are larger than those of the AAO over the period 1984–1994. This period corresponds to the years of sea ice propagation, whereas in the

nonpropagating years (1979–1983 and 1995–2003), variances of the AAO are more pronounced than those of the PSA pattern. Moreover, Figure 10 demonstrates that the atmospheric shift of the dominant pattern occurred several times from the 1960s to the 2000s: in the mid-1970s, -1980s, and -1990s.

[27] Consequently, the amplitude and frequency shifts of the PSA pattern, as well as the amplitude shift of the AAO, determine whether the SIC propagates. These shifts of atmospheric patterns cause the modulation in sea ice variation patterns in the Southern Ocean. The viewpoint of sea ice modulation enabled us to clarify the presence of the shifts of the AAO and the PSA pattern.

6. Concluding Remarks

[28] We investigated the interannual variation in SIC anomalies around the Antarctic using an EOF analysis for newly available passive satellite-derived microwave data for the period of 1979–2003. The period of eastward propagation was only from 1984 to 1994, with no significant eastward propagating features of the SIC in other years. This large modulation in the SIC suggests that the change of a climate variability occurred. We also clarified the difference in dominant large-scale atmospheric patterns in association with the SIC modulation. In the nonpropagating years, the variance of tropospheric AAO was predominant. In the rotating years, the variance of the PSA pattern with a 4 year cycle in the troposphere was predominant, whereas AAO variance was subdominant. Such predominant periodic atmospheric external forcing allows the SIC to propagate eastward.

[29] The causes of the modulation in the SIC pattern include the amplitude and frequency shifts of large-scale atmospheric variability. The switch in the dominant atmospheric pattern from the PSA to the AAO in the mid-1990s is synchronized with the modulation in the SIC pattern. In addition, we can demonstrate that the shift of the dominant atmospheric pattern between the AAO and PSA occurred in the mid-1970s, -1980s, and -1990s. It is known that the PSA pattern is influenced by ENSO [e.g., *Karoly*, 1989; *Trenberth et al.*, 1998; *Kidson*, 1999]. However, no significant modulations of the ENSO cycle occurred in the mid-1970s, -1980s, and -1990s. This suggests that the response of the high-latitude atmosphere to quasi-cyclic tropical forcing is not simple. The causes of long-term shift of the AAO also require further research. Because the AAO and the PSA are hemispheric-scale atmospheric phenomena, these shifts may influence other climatic subsystems.

[30] **Acknowledgments.** We extend our thanks to S. Aoki, K. Ohshima, and Y. Fukamachi for their useful advice. Our thanks go to the reviewers and the Editor; without their helpful suggestions, this paper could not have been accomplished. The Grid Analysis and Display System (GrADS) was used to draw the figures.

References

Bonekamp, H., A. Sterl, and G. J. Komen (1999), Interannual variability in the Southern Ocean from an ocean model forced by European Center for Medium-Range Weather Forecasts reanalysis fluxes, *J. Geophys. Res.*, *104*(C6), 13,317–13,331, doi:10.1029/1999JC900052.

Bromwich, D. H., and R. L. Fogt (2004), Strong trends in the skill of the ERA-40 and NCEP-NCAR reanalyses in the high and middle latitudes of the Southern Hemisphere, 1958–2001, *J. Clim.*, *17*, 4603–4619, doi:10.1175/3241.1.

Bromwich, D. H., R. L. Fogt, K. I. Hodges, and J. E. Walsh (2007), A tropospheric assessment of the ERA-40, NCEP, and JRA-25 global reanalyses in the polar regions, *J. Geophys. Res.*, *112*, D10111, doi:10.1029/2006JD007859.

Cai, W., and P. G. Baines (2001), Forcing of the Antarctic Circumpolar Wave by El Niño-Southern Oscillation teleconnections, *J. Geophys. Res.*, *106*(C5), 9019–9038, doi:10.1029/2000JC000590.

Cai, W., and I. G. Watterson (2002), Modes of interannual variability of the Southern Hemisphere circulation simulated by the CSIRO climate model, *J. Clim.*, *15*, 1159–1174, doi:10.1175/1520-0442(2002)015<1159:MOIVOT>2.0.CO;2.

Cavalieri, D., C. Parkinson, P. Gloersen, and H. J. Zwally (1996), Sea ice concentrations from Nimbus-7 SMMR and DMSP SSM/I passive microwave data, http://nsidc.org/data/nsidc-0051.html, Natl. Snow and Ice Data Cent., Boulder, Colo. (Updated 2008.)

Cavalieri, D. J., P. Gloerson, C. L. Parkinson, J. C. Comiso, and H. J. Zwally (1997), Observed hemispheric asymmetry in global sea ice change, *Science*, *278*, 1104–1106, doi:10.1126/science.278.5340.1104.

Connolley, W. M. (2002), Long-term variation of the Antarctic Circumpolar Wave, *J. Geophys. Res.*, *107*, 8076, doi:10.1029/2000JC000380, [printed 108(C4), 2003].

Gloersen, P., and W. B. White (2001), Reestablishing the circumpolar wave in sea ice around Antarctica from one winter to the next, *J. Geophys. Res.*, *106*(C3), 4391–4395, doi:10.1029/2000JC000230.

Gong, D.-Y., and S.-W. Wang (1999), Definition of Antarctic oscillation index, *Geophys. Res. Lett.*, *26*(4), 459–462, doi:10.1029/1999GL900003.

Holland, M. M., C. M. Bitz, and E. C. Hunke (2005), Mechanisms forcing an Antarctic dipole in simulated sea ice and surface ocean conditions, *J. Clim.*, *18*, 2052–2066, doi:10.1175/JCLI3396.1.

Hoskins, B. J., and D. J. Karoly (1981), The steady linear response of a spherical atmosphere to thermal and orographic forcing, *J. Atmos. Sci.*, *38*, 1179–1196, doi:10.1175/1520-0469(1981)038<1179:TSLROA>2.0.CO;2.

Jacobs, G. A., and J. L. Mitchell (1996), Ocean circulation variations associated with the Antarctic Circumpolar Wave, *Geophys. Res. Lett.*, *23*(21), 2947–2950, doi:10.1029/96GL02492.

Kalnay, E., et al. (1996), The NCEP/NCAR 40-year reanalysis project, *Bull. Am. Meteorol. Soc.*, *77*, 437–471, doi:10.1175/1520-0477(1996)077<0437:TNYRP>2.0.CO;2.

Karoly, D. J. (1989), Southern Hemisphere circulation features associated with El Niño–Southern Oscillation events, *J. Clim.*, *2*, 1239–1252, doi:10.1175/1520-0442(1989)002<1239:SHCFAW>2.0.CO;2.

Kidson, J. W. (1999), Principal modes of Southern Hemisphere low-frequency variability obtained from NCEP-NCAR reanalyses, *J. Clim.*, *12*, 2808–2830, doi:10.1175/1520-0442(1999)012<2808:PMOSHL>2.0.CO;2.

Kidson, J. W., and J. A. Renwick (2002), The Southern Hemisphere evolution of ENSO during 1981–1999, *J. Clim.*, *15*, 847–863, doi:10.1175/1520-0442(2002)015<0847:TSHEOE>2.0.CO;2.

Kwok, R., and J. C. Comiso (2002), Southern Ocean climate and sea ice anomalies associated with the Southern Oscillation, *J. Clim.*, *15*, 487–501, doi:10.1175/1520-0442(2002)015<0487:SOCASI>2.0.CO;2.

Martinson, D. G. (1993), Ocean heat and seasonal sea ice thickness in the Southern Ocean, in *The Climate System*, vol. 12, edited by W. R. Peltier, pp. 597–609, Springer, New York.

Mo, K. C. (2000), Relationships between low-frequency variability in the Southern Hemisphere and sea surface temperature anomalies, *J. Clim.*, *13*, 3590–3610.

Mo, K. C., and M. Ghil (1987), Statistics and dynamics of persistent anomalies, *J. Atmos. Sci.*, *44*, 877–902.

Motoi, T., A. Kito, and H. Koide (1998), Antarctic Circumpolar Wave in a coupled ocean-atmosphere model, *Ann. Glaciol.*, *27*, 483–487.

Park, Y.-H., F. Roquet, and F. Vivier (2004), Quasi-stationary ENSO wave signals versus the Antarctic Circumpolar Wave scenario, *Geophys. Res. Lett.*, *31*, L09315, doi:10.1029/2004GL019806.

Qiu, B., and F. Jin (1997), Antarctic circumpolar waves: An indication of ocean-atmosphere coupling in the extratropics, *Geophys. Res. Lett.*, *24*(21), 2585–2588, doi:10.1029/97GL02694.

Raphael, M. N. (2004), A zonal wave 3 index for the Southern Hemisphere, *Geophys. Res. Lett.*, *31*, L23212, doi:10.1029/2004GL020365.

Raphael, M. N. (2007), The influence of atmospheric zonal wave three on Antarctic sea ice variability, *J. Geophys. Res.*, *112*, D12112, doi:10.1029/2006JD007852.

Rasmusson, E. M., X. Wang, and C. F. Ropelewski (1990), The biennial component of ENSO variability, *J. Mar. Syst.*, *1*, 71–96, doi:10.1016/0924-7963(90)90153-2.

Renwick, J. A. (2002), Southern Hemisphere circulation and relationships with sea ice and sea surface temperature, *J. Clim.*, *15*, 3058–3068, doi:10.1175/1520-0442(2002)015<3058:SHCARW>2.0.CO;2.

Renwick, J. A., and M. J. Revell (1999), Blocking over the South Pacific and Rossby wave propagation, *Mon. Weather Rev.*, *127*, 2233–2247, doi:10.1175/1520-0493(1999)127<2233:BOTSPA>2.0.CO;2.

Reynolds, R. W., and T. M. Smith (1994), Improved global sea surface temperature analyses using optimum interpolation, *J. Clim.*, *7*, 929–948, doi:10.1175/1520-0442(1994)007<0929:IGSSTA>2.0.CO;2.

Tennant, W. (2004), Considerations when using pre-1979 NCEP/NCAR reanalyses in the Southern Hemisphere, *Geophys. Res. Lett.*, *31*, L11112, doi:10.1029/2004GL019751.

Thompson, D. W. J., and J. M. Wallace (2000), Annular modes in the extratropical circulation. Part I: Month-to-month variability, *J. Clim.*, *13*, 1000–1016, doi:10.1175/1520-0442(2000)013<1000:AMITEC>2.0.CO;2.

Trenberth, K. E., G. W. Branstator, D. Karoly, A. Kumar, N.-C. Lau, and C. Ropelewski (1998), Progress during TOGA in understanding and modeling global teleconnections associated with tropical sea surface temperatures, *J. Geophys. Res.*, *103*(C7), 14,291–14,324, doi:10.1029/97JC01444.

White, W. B., and R. G. Peterson (1996), An Antarctic Circumpolar Wave in surface pressure, wind, temperature and sea-ice extent, *Nature*, *380*, 699–702, doi:10.1038/380699a0.

White, W. B., S.-C. Chen, and R. G. Peterson (1998), The Antarctic Circumpolar Wave: A beta effect in ocean-atmosphere coupling over the Southern Ocean, *J. Phys. Oceanogr.*, *28*, 2345–2361, doi:10.1175/1520-0485(1998)028<2345:TACWAB>2.0.CO;2.

Yuan, X. (2004), ENSO-related impacts on Antarctic sea ice: A synthesis of phenomenon and mechanisms, *Antarct. Sci.*, *16*, 415–425, doi:10.1017/S0954102004002238.

Yuan, X., and D. G. Martinson (2000), Antarctic sea ice variability and its global connectivity, *J. Clim.*, *13*, 1697–1717, doi:10.1175/1520-0442(2000)013<1697:ASIEVA>2.0.CO;2.

Yuan, X., and D. G. Martinson (2001), The Antarctic dipole and its predictability, *Geophys. Res. Lett.*, *28*(18), 3609–3612, doi:10.1029/2001GL012969.

Y. Tachibana, Research Institute for Global Change, JAMSTEC, 2-15 Natsushima-cho Yokosuka, Kanagawa 237-0061, Japan. (tachi@bio.mie-u.ac.jp)

Y. Udagawa, Graduate School of Environmental Science, Hokkaido University, North 10 West 5, Kita-ku, Sapporo, Hokkaido 060-0810, Japan. (udagawa@ees.hokudai.ac.jp)

Y. Yamazaki, Faculty of Environmental Earth Science, Hokkaido University, Kita-ku, Sapporo, Hokkaido 060-0810, Japan. (yamazaki@ees.hokudai.ac.jp)